PHYSICAL REVIEW D **76,** 105017 (2007)

Cosmological constraints on neutrino injection

Toru Kanzaki and Masahiro Kawasaki
Institute for Cosmic Ray Research, University of Tokyo, Kashiwa 277-8582, Japan

Kazunori Kohri
Physics Department, Lancaster University, Lancaster LA1 4YB, United Kingdom

Takeo Moroi
Department of Physics, Tohoku University, Sendai 980-8578, Japan
(Received 5 June 2007; published 16 November 2007)

We derive general constraints on the relic abundances of a long-lived particle which mainly decays into a neutrino (and something else) at cosmological time scales. Such an exotic particle may show up in various particle-physics models based on physics beyond the standard model. The constraints are obtained from big bang nucleosynthesis, cosmic microwave background, and diffuse neutrino and photon fluxes, depending on the lifetime and the electromagnetic and hadronic branching ratios.

DOI: 10.1103/PhysRevD.76.105017 PACS numbers: 14.80.−j, 26.35.+c, 95.85.Ry, 98.70.Vc

I. INTRODUCTION

In modern cosmology, the success of the big bang nucleosynthesis (BBN) and existence of the cosmic microwave background (CMB) are important facts that support the standard big bang model. Prediction of the standard BBN scenario is in reasonable agreement with the observations, and the COBE observations [1] showed the perfect blackbody of CMB spectrum. On the other hand, in particle physics, if we consider physics beyond the standard model, there exist various new particles, some of which have long lifetimes and decay during or after BBN. Examples of such long-lived particles include the gravitino and moduli predicted in the framework of supersymmetry and string theories.

BBN and CMB are useful probes to exotic particles predicted in physics beyond the standard model. In fact, the prediction of BBN changes significantly if there exists an exotic massive particle with long lifetime. (Hereafter, we call such a particle X.) When the lifetime of X is longer than about 1 sec., the decay of X may induce electromagnetic and hadronic showers, which lead to photo- and hadro-dissociation of ^{4}He and subsequent nonthermal production of other light elements (D, ^{3}He, ^{6}Li, and ^{7}Li). Such processes may significantly change the prediction of the standard BBN scenario and, consequently, resultant abundances of light elements may conflict with observations. Furthermore, the electromagnetic energy injection causes distortion of the CMB spectrum. Since the observation [1] shows that this distortion is quite small, we can constrain the abundance of X. Finally, if the lifetime is very long, the spectrum of neutrinos and photons produced by the decay of X are not thermalized and may be directly observed.

The effects of the long-lived particles on BBN were well-studied for radiative decay [2–5] and for hadronic decay [6–12] and stringent constraints on the abundance and lifetime of X were obtained. However, when X mainly decays into neutrinos, it is expected that the constraints become much weaker because of the weakness of interactions between neutrinos and other standard-model particles. The specific case where a sneutrino mainly decays into a gravitino and a neutrino has been already discussed in [13–15]. Such a scenario is realized when the sneutrino is the next lightest superparticle (NLSP) while the gravitino is the lightest superparticle (LSP).[1] In such a case, interaction of X (i.e., sneutrino) is well-known, and it is found that BBN provides the most stringent constraint.

However, there are other possibilities of having long-lived massive particles which dominantly decay into neutrinos. For example, if the LSP is axino ($\tilde{a}$) and the NLSP is sneutrino, the dominant decay process of the sneutrino ($=$ X) is $\tilde{\nu} \to \nu + \tilde{a}$. The decay rate of this process depends on the properties of axion supermultiplet. Thus, in general, properties of X (i.e., lifetime, hadronic branching ratio, and so on) are model-dependent. Consequently, the most stringent bound may not be from BBN. For example, high-energy neutrinos emitted in the X particle decay were considered in [16] where the upper bounds on the X abundance were obtained from nucleon-decay detectors and fly's eye air shower array.

In this paper, we derive general cosmological constraints on scenarios in which there exists a long-lived massive particle which dominantly decays into a neutrino (and something else). We treat the lifetime and hadronic branching ratio of the long-lived particle as free parameters. In this case, in fact, the constraint from the main decay mode is quite weak, and other subdominant decay channels which contain electronic and hadronic particles may be important [15]. In our analysis, we take into account both

[1]For the case that the gravitino is the NLSP and the sneutrino is the LSP, see also [13].

of these decay channels and discuss various cosmological constraints.

Organization of this paper is as follows. In Sec. II, we discuss BBN constraints. In Sec. III, constraints from CMB are considered. Then in Sec. IV, we study constraints from diffuse neutrino and photon. Sec. V is devoted to conclusions.

II. BBN CONSTRAINTS

Before going into the main subject of this section, which is the constraints from the BBN, let us first summarize the properties of the long-lived heavy particle X which mainly decays into a neutrino (and some other weakly interacting particle). In our study, we assume that X mainly decays as

$$X \to \nu + Y, \tag{1}$$

where Y is an invisible particle which is very weakly interacting so that it does not cause any subsequent scattering with background particles. One of the well-motivated examples is the case where the sneutrino is the NLSP while gravitino (or axino) is the LSP. (Then, X is the sneutrino and Y is the gravitino or axino.) In addition, for concreteness, we assume that the final-state neutrino is an electron neutrino. (We note here that we have checked that the constraints on the properties of X are not sensitive to the flavor of the final-state neutrino.)

Even though the dominant decay mode is the two-body process, one should keep in mind that decay channels with three- and/or four-body final states should also exist since the neutrino as well as X and/or Y couple to Z- and W-bosons. The emitted (real or virtual) weak bosons subsequently decay into quarks and leptons. With this type of three- and/or four-body decay processes, energetic quarks and charged leptons are produced.

If the decays of X occur during or after BBN, the standard-model particles emitted in the decay can affect the abundances of primordial light elements. First, the high-energy neutrinos emitted in the main decay mode (two-body decay) scatter off the background leptons and produce charged leptons ($e^{\pm}$, $\mu^{\pm}$) and charged pions. The former induce electromagnetic showers which destroy light elements, and the latter change the n-p ratio through nucleon and pion interactions. Second, X decays into electromagnetic and hadronic particles via the three- and/or four-body decay modes with small branching ratio B_X. Such processes directly induce electromagnetic and hadronic showers and change the abundances of light elements [10].

A. Two-body decay

First, we discuss effects of the dominant decay process $X \to Y + \nu_e$. We presume that Y produced in the decay is a very weakly interacting particle, and that it is irrelevant for BBN. The neutrino, however, may affect abundances of light elements. The emitted energetic neutrinos scatter off background leptons via weak interaction and several kinds of particles may be pair-produced.

First, charged leptons may be produced via the following processes[2]:

$$\nu_i + \bar{\nu}_{i,\mathrm{BG}} \to e^- + e^+, \tag{2}$$

$$\nu_i + \bar{\nu}_{i,\mathrm{BG}} \to \mu^- + \mu^+, \tag{3}$$

$$\nu_\mu + \bar{\nu}_{e,\mathrm{BG}} \to \mu^- + e^+, \tag{4}$$

$$\nu_e + \bar{\nu}_{\mu,\mathrm{BG}} \to e^- + \mu^+, \tag{5}$$

where $i = e, \mu, \tau$ is the flavor index, and the subscript BG is for background particles. The muons emitted in the above processes quickly decay into electrons and neutrinos. Thus, the above processes produce energetic electrons and positrons which cause electromagnetic cascade. Energetic photons in the cascade induce photo-dissociation processes of light elements. The effects of these processes have been already studied in [13].

Another possible effect is due to the production of pion pairs. High-energy neutrinos scatter off the background neutrinos and electrons (positrons) and produce pions as

$$\nu_i + \bar{\nu}_{i,\mathrm{BG}} \to \pi^- + \pi^+, \tag{6}$$

$$\nu_i + e^{\pm}_{i,\mathrm{BG}} \to \pi^0 + \pi^{\pm}. \tag{7}$$

The nucleus-pion interaction rate is $\sim 10^8\ \mathrm{sec}^{-1} \times (T/\mathrm{MeV})^3$, which is larger than the decay rate of the charged pion ($\sim 4 \times 10^7\ \mathrm{sec}^{-1}$) for $T \sim 1$ MeV. Therefore, the charged pions produced at $T \sim 1$ MeV scatter off the background nuclei and change protons (neutrons) into neutrons (protons) via

$$\pi^- + p \to n + \pi^0, \qquad n + \gamma, \tag{8}$$

$$\pi^+ + n \to p + \pi^0, \qquad p + \gamma. \tag{9}$$

Consequently, the n/p ratio is increased, resulting in more ^{4}He. Notice that, because of very short lifetime, the neutral pions decay before they scatter off the background nuclei. Thus, they do not induce $p \leftrightarrow n$ conversion. Effects of the photo-dissociation processes by the photons from π^0 is induced in our analysis.

In order to estimate effects of the high-energy-neutrino induced processes, we have numerically solved the Boltzmann equation describing the time evolution of the high-energy-neutrino spectrum taking into account all of

[2]Neutrinos may also scatter off the background electron and positron. However, the photo-dissociation processes become important when the cosmic temperature becomes much lower than 1 MeV. At such temperature, number densities of electrons and positrons are extremely suppressed, and hence the scattering processes with electrons and positrons are irrelevant for the production of charged leptons.

the processes above. Details of our calculation are given in Appendix A.

B. Three- and four-body decay

Even though the branching ratio for three- and four-body decay processes are much smaller than 1, such decay processes are very important since quarks, gluons, and charged particles are directly emitted from these decay processes. Energetic quarks, gluons, and charged particles may significantly change the prediction of the standard BBN scenario. Effects of these particles are classified into three categories: photo-dissociations, hadro-dissociations, and $p \leftrightarrow n$ conversion.

In order to study the effects of three- and four-body decay processes, it is important to obtain the spectra of quarks and leptons emitted by the decay of X, which depends on the model. In our analysis, we use, up to normalization, those obtained in the case where X is the sneutrino and Y is the gravitino; in such a case, the sneutrino may decay into the gravitino, neutrino (or charged lepton), and $Z^{(*)}$ (or $W^{(*)}$), and the produced (real or virtual) weak bosons subsequently decay into a quark- or lepton-pair. (Here, Z^* and W^* denote virtual weak bosons.) In order to perform our analysis in as model-independent a way as possible, we treat the branching ratio for three- and four-body processes as a free parameter: we define the branching ratio B_X as

$$B_X \equiv \frac{\Gamma(X \to 3\,\text{body}) + \Gamma(X \to 4\,\text{body})}{\Gamma(X \to \text{all})}, \tag{10}$$

where Γ is decay width. For the study of the effects of photo-dissociation processes and CMB spectral distortion, we also calculate the averaged "visible energy" emitted from one X:

$$E_{\text{vis}} = B_X \langle E_{\text{vis}} \rangle, \tag{11}$$

$$\langle E_{\text{vis}} \rangle = \frac{\sum_{i:\ 3,4\text{-body}} E_i(\gamma, l^{\pm}) \times \Gamma_i}{\sum_{i:\ 3,4\text{-body}} \Gamma_i}, \tag{12}$$

where $E_i(\gamma, l^{\pm})$ is the averaged energy carried away by charged particles and photons in each of the three- and four-decay modes. The energy distributions of photons, neutrinos, leptons, and nucleons produced by the decay of X are calculated by means of Monte Carlo simulations with the PYTHIA package [17]. In Fig. 1, we plot the spectra of photons and leptons ($e^+ + e^-$), respectively. From these distributions we calculate the averaged energy and obtain $\langle E_{\text{vis}} \rangle = 25.3$, 146, 821, and 5630 GeV for $m_X = 10^2$, 10^3, 10^4, and 10^5 GeV, respectively. Here, m_X is the mass of X. E_{vis} is much smaller than m_X since we are interested in the case where $B_X \ll 1$.

Photo-dissociation processes are induced by energetic photons in an electromagnetic shower which is caused by charged particles and/or photons emitted from X. With a given background temperature, the distribution function of energetic photons depends on the total amount of energy injected by particles with electromagnetic interaction, and is insensitive to the shape of the energy spectrum of primary particles. Thus, once E_{vis} is obtained, the energy distribution of energetic photons in the electromagnetic shower can be obtained. Then, photo-dissociation rates are obtained by convoluting the energy distribution function and cross sections of photo-dissociation reactions. For

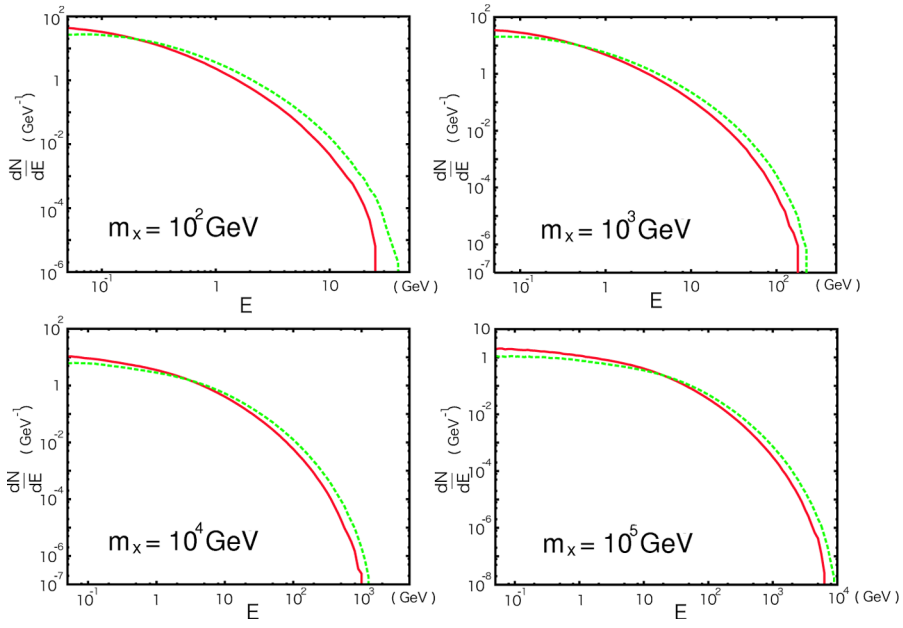

FIG. 1 (color online). Spectrum of $e^+ + e^-$ (solid line) and photon (dashed line) with $m_X = 10^2$ GeV $- 10^5$ GeV.

details of our treatment of photo-dissociation processes, see [3].

For the study of hadro-dissociation processes, it is necessary to obtain energy distributions of (primary) hadrons which are produced after the hadronization of quarks emitted from X. We have calculated the spectra of p and n by using PYTHIA. These hadrons cause hadronic showers and induced hadro-dissociation processes. In our analysis, in addition, we have also calculated the number of charged pions produced by the decay of X. Such charged pions, protons, and neutrons become the source of $p \leftrightarrow n$ conversion processes, which changes the number of ^{4}He [7,9].[3] Once the spectra of hadrons are obtained, effects of hadro-dissociation and $p \leftrightarrow n$ conversion are studied with the procedure given in [10].

C. Numerical results

In our analysis, we have followed the evolutions of the number densities of the light elements. For this purpose, we have modified the Kawano code [18] including photo- and hadro-dissociation processes. As observational constraints on the primordial abundances of light elements, we adopt those used in [15] except for $Y_{\rm p}$ and $(n_{^3{\rm He}}/n_{\rm D})_{\rm p}$:

$$(n_{\rm D}/n_{\rm H})_{\rm p} = (2.82 \pm 0.26) \times 10^{-5}, \tag{13}$$

$$(n_{^3{\rm He}}/n_{\rm D})_{\rm p} < 0.83 + 0.27, \tag{14}$$

$$Y_{\rm p} = 0.2516 \pm 0.0040, \tag{15}$$

$$\log_{10}(n_{^7{\rm Li}}/n_{\rm H})_{\rm p} = -9.63 \pm 0.06 \pm 0.3. \tag{16}$$

$$(n_{^6{\rm Li}}/n_{^7{\rm Li}})_{\rm p} < 0.046 \pm 0.022 + 0.084, \tag{17}$$

where the subscript "p" is for primordial value (just after BBN), and $Y_{\rm p}$ is the primordial mass fraction of ^{4}He. For the center value of $Y_{\rm p}$, we have adopted the value reported in [19] in which the authors used new data of HeI emissivities,[4] and conservatively added a larger error ($= 0.0040$) as discussed in [21]. For $(n_{^3{\rm He}}/n_{\rm D})_{\rm p}$, we have adopted most newly-reported values of D and ^{3}He abundances observed in protosolar clouds [22], $(n_{^3{\rm He}}/n_{\rm H})_{\rm PSC} = (1.66 \pm 0.06) \times 10^{-5}$ and $(n_{\rm D}/n_{\rm H})_{\rm PSC} = (2.00 \pm 0.35) \times 10^{-5}$, where the subscript "PSC" means a value in the protosolar cloud. (For the importance of the upper bounds on $(n_{^3{\rm He}}/n_{\rm D})_{\rm p}$, see [10,23].)

We parametrize the primordial abundance of X by yield variable Y_X which is defined as the ratio of number density and total entropy density at ($t \ll \tau_X$):

[3]Here we have neglected the effects of Kaons to the $p \leftrightarrow n$ conversion, according to the discussion in [10].

[4]See also the other recent value of $Y_{\rm p}$ reported in [20] where the authors adopted larger errors (0.0028) than that of [19].

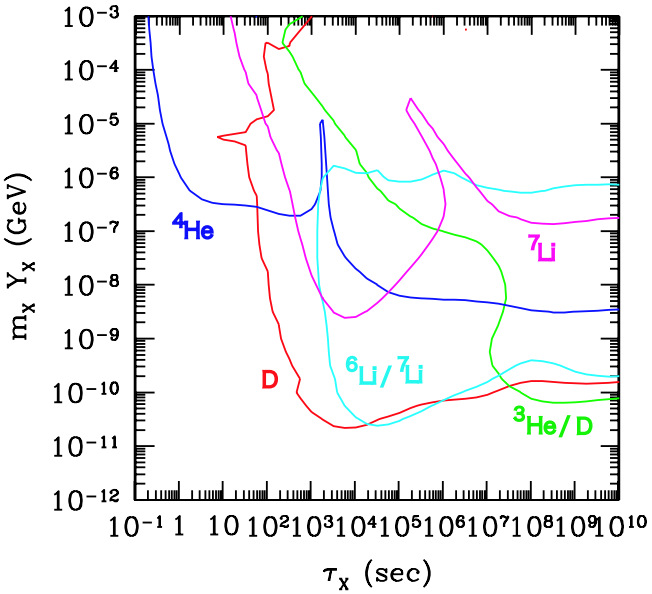

FIG. 2 (color online). BBN constraints on τ_X vs. $m_X Y_X$ plane. Here, we take $m_X = 100$ GeV and $B_X = 10^{-3}$. These lines are upper bounds deduced from observations.

$$Y_X \equiv \left[\frac{n_X}{s}\right]_{t \ll \tau_X}, \tag{18}$$

where τ_X is the lifetime of X. Here, we consider the case where X is decoupled from the thermal bath. In addition, we assume that the effect of the entropy production is negligible. Thus, Y_X is (almost) a constant of time when $t \ll \tau_X$. If Y_X is too large, abundances of light elements are too much affected to be consistent with the observations. Thus, we can derive upper bound on Y_X.

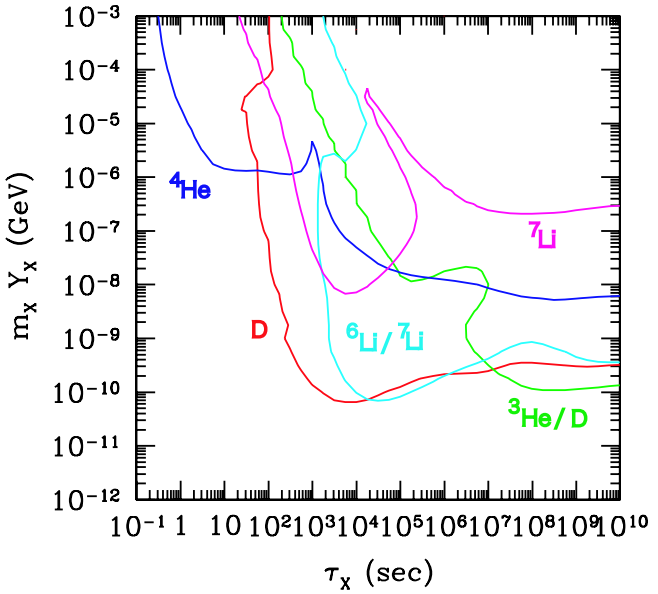

FIG. 3 (color online). BBN constraints on τ_X vs. $m_X Y_X$ plane. Here, we take $m_X = 1$ TeV and $B_X = 10^{-3}$.

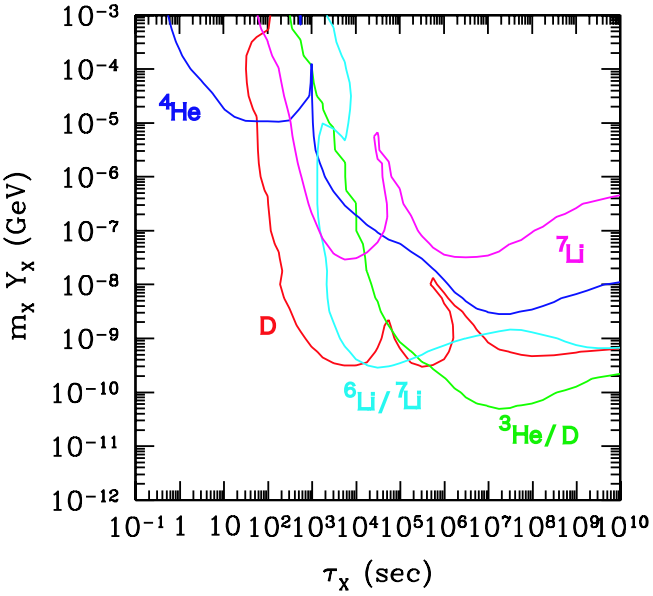

FIG. 4 (color online). BBN constraints on τ_X vs. $m_X Y_X$ plane. Here, we take $m_X = 10$ TeV and $B_X = 10^{-3}$.

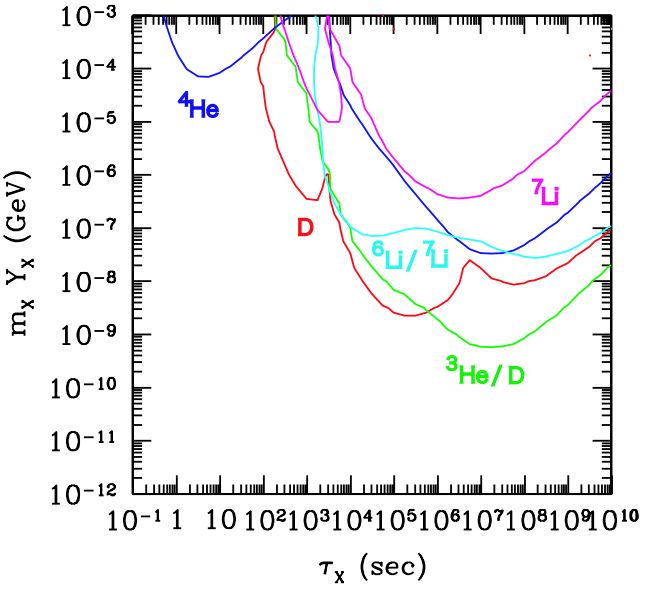

FIG. 6 (color online). BBN constraints on τ_X vs. $m_X Y_X$ plane. Here, we take $m_X = 1$ TeV and $B_X = 10^{-6}$.

In Figs. 2–7, we show BBN constraints on τ_X and $m_X Y_X$ for $B_X = 10^{-3}$ and $B_X = 10^{-6}$; we found that constraints with $B_X = 0$ are almost the same as those with $B_X = 10^{-6}$.

As one can see from these figures, the most important constraint comes from overproduction of ^{4}He when $\tau_X \lesssim 10^2$ sec. Since protons are more abundant than neutrons, a significant amount of proton may be converted to neutron through nucleus-pion interaction (and nucleon-nucleon interactions for relatively large B_X) and consequently ^{4}He is overproduced. When 10^2 sec $\lesssim \tau_X \lesssim 10^7$ sec, the background ^{4}He (which we call $\alpha_{\rm BG}$) is effectively dissociated by the energetic hadrons produced in the hadronic shower. In this case, overproduction of D may occur as a result of hadro-dissociation of $\alpha_{\rm BG}$. In addition, energetic T and ^{3}He are also produced and they synthesize ^{6}Li through the ^{6}Li via $\mathrm{T} + \alpha_{\rm BG} \to {}^6\mathrm{Li} + n$ and ${}^3\mathrm{He} + \alpha_{\rm BG} \to {}^6\mathrm{Li} + p$. When $\tau_X \gtrsim 10^7$ sec, the energetic hadrons are stopped by the scattering processes with background electrons, and hence the effects of hadro-dissociation become less efficient than those of the photo-dissociation. In particular, the

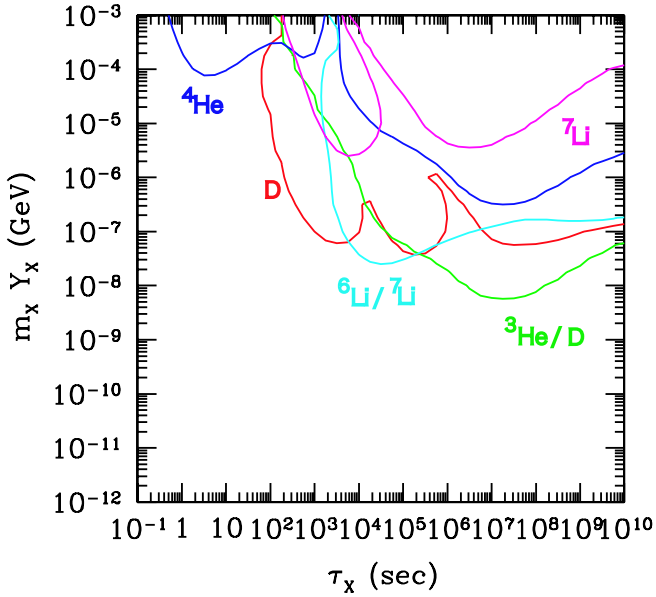

FIG. 5 (color online). BBN constraints on τ_X vs. $m_X Y_X$ plane. Here, we take $m_X = 100$ GeV and $B_X = 10^{-6}$.

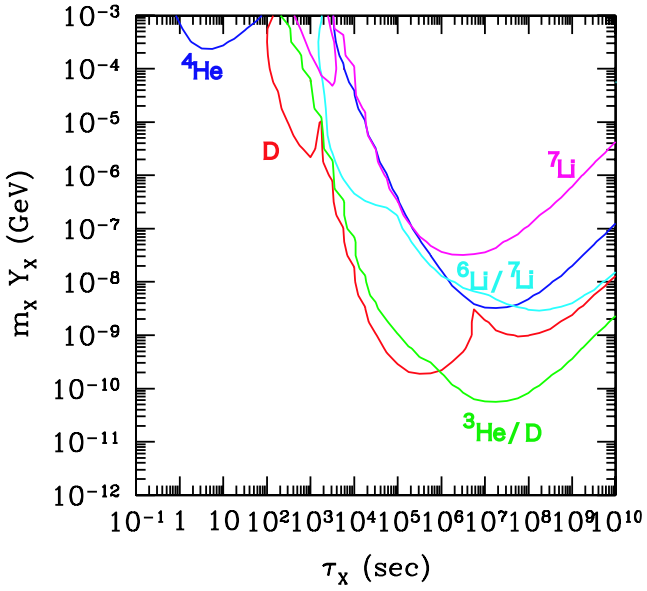

FIG. 7 (color online). BBN constraints on τ_X vs. $m_X Y_X$ plane. Here, we take $m_X = 10$ TeV and $B_X = 10^{-6}$.

energetic photons produced in the electromagnetic shower destroy $\alpha_{\rm BG}$. In this case, overproduction of D and ^{3}He occurs as a result of photo-dissociation of $\alpha_{\rm BG}$.

The constraints on $m_X Y_X$ depend on m_X in a nontrivial way. The constraint coming from the photo-dissociation caused by the two-body decay becomes stringent as m_X increases because neutrinos emitted in two-body decay have higher energy and scatter off the background neutrinos with larger rate. On the other hand, the rates of the hadro-dissociation and photo-dissociation caused by the three- and four-body decay depend only on $E_{\rm vis} Y_X$ and hence the constraints on $m_X Y_X$ become slightly milder as m_X increases. The constraint from $n \leftrightarrow p$ conversion becomes weaker as m_X increases. This is because the charged pion production is roughly determined by Y_X for the three- and four-body decay.

So far, we have shown the results for the case where the primary neutrino is electron-type. However, we have checked that the BBN constraints are almost unchanged even if X decays into a muon or tau neutrino (and Y).

III. CMB CONSTRAINTS

CMB also imposes constraints on the decays of X. COBE observations show that the CMB spectrum is almost perfect blackbody [1]. Therefore any exotic energy injections that cause distortions in the spectrum of CMB are stringently constrained [24–26]. When the photons are emitted before redshift $z \sim 10^7$, they are thermalized by Compton scattering, double Compton scattering, and bremsstrahlung, and no spectral distortion takes place. However, at $z \lesssim 10^7$ only Compton scattering is efficient. Since the Compton scattering does not change the total number of photons, the resultant spectrum becomes a Bose-Einstein distribution with a finite chemical potential μ, regardless of the detail of the injection. For the case of massive particle decay, the number density of injected photons is negligible compared with that in the background. Therefore, the spectral distortions are determined by the fraction of the energy release, $\Delta\rho_\gamma/\rho_\gamma$. Then, for small $\Delta\rho_\gamma/\rho_\gamma$ the chemical potential of the photon spectrum is given by

$$\mu \simeq \frac{1}{0.714}\frac{\Delta\rho_\gamma}{\rho_\gamma}. \tag{19}$$

As we have discussed, there are two types of processes which contribute to the electromagnetic energy injection ($\Delta\rho_\gamma$) in the present scenario. One is the two-body decay process: the high-energy primary neutrinos emitted by X scatter off the background neutrinos and create charged leptons whose energy is finally converted to the energy of radiation. The other is the three- and four-body decay processes by which quarks and charged leptons are produced. In our analysis, we have taken into account both of these contributions.

A. Three and four-body decay

There are two quantities which are required to calculate the electromagnetic energy injection: branching ratio B_X and the averaged energy $\langle E_{\rm vis}\rangle$.

We follow the treatment of [26] for the case of three- and four-body decays. Using the fact that X decays exponentially in time with lifetime τ_X, we obtain

$$\frac{\Delta\rho_\gamma}{\rho_\gamma} = \frac{\langle E_{\rm vis}\rangle}{2.701 T(t_{\rm eff})}\frac{n_X}{n_\gamma}B_X, \tag{20}$$

where $T(t)$ is the CMB temperature and n_X is the number density of X before decay. Here $t_{\rm eff} = [\Gamma(1+\beta)]^{1/\beta}\tau_X$ for time-temperature relation $T \propto t^{-\beta}$, where Γ is the gamma function.

From Eqs. (19) and (20), we find that the chemical potential is given by

$$\mu \simeq 4.00 \times 10^2 \left(\frac{\tau_X}{1\ \text{sec}}\right)^{1/2}\left(\frac{\langle E_{\rm vis}\rangle}{1\ \text{GeV}}\right)B_X\frac{n_X}{n_\gamma}. \tag{21}$$

We have assumed here that we are in the radiation dominated epoch where $T \propto t^{-1/2}$. Note that, however, photon-number changing processes (double Compton scattering and bremsstrahlung) become increasingly efficient as the photon frequency decreases. This means the spectrum becomes blackbody at low frequencies. The photons with low frequencies produced by the photon-number changing processes are transferred to higher frequencies by inverse Compton scattering and the chemical potential decreases in time. For a low $\Omega_b h^2$ Universe suggested by BBN [27] and WMAP [28] (where, in this paper, Ω_b denotes the density parameter of baryon, and h is the Hubble constant in units of 100 km/sec/Mpc), double Compton scattering dominates the thermalization process. The chemical potential produced at $t = t_h$ is blurred out at an exponential rate and the present value is given by [29]

$$\mu_0 \equiv \mu(t_0) = \mu(t_h)\exp(-(t_{\rm DC}/t_h)^{5/4}) \tag{22}$$

with

$$t_{\rm DC} = 6.81 \times 10^6 \left(\frac{\Omega_b h^2}{0.0223}\right)^{4/5}\left(1 - \frac{Y_p}{2}\right)^{4/5}\ \text{sec}. \tag{23}$$

Combining Eq. (21) with Eq. (22), we find that the chemical potential today is given by [26]

$$\mu_0 \simeq 4.00 \times 10^2 \left(\frac{\tau_X}{1\ \text{sec}}\right)^{1/2}\exp(-(t_{\rm DC}/\tau_X)^{5/4}) \times \left(\frac{\langle E_{\rm vis}\rangle}{1\ \text{GeV}}\right)B_X\frac{n_X}{n_\gamma}. \tag{24}$$

For late energy injection ($z \lesssim 10^5$), Compton scattering can no longer establish the Bose-Einstein distribution. In this case, the spectrum can be described by the Compton y-parameter which is defined by

$$y = \int dt \frac{T_e - T}{m_e} n_e \sigma_T, \tag{25}$$

where m_e and T_e are the number density and temperature of electrons and σ_T is Thomson cross section. Then the energy injection is related to y as $\Delta\rho_\gamma/\rho_\gamma = 4y$. Here, we define z_K as the redshift at which the time scale for energy exchange through Compton scatterings is equal to the Hubble time;

$$z_K \simeq 4.77 \times 10^4 \left(\frac{\Omega_b h^2}{0.0223}\right)^{-1/2} \left(1 - \frac{Y_p}{2}\right)^{-1/2}. \tag{26}$$

The spectrum can be described by chemical potential μ for energy injection at $z > z_K$ and by Compton y-parameter for energy injection at $z < z_K$. Here we take $\Omega_b h^2 = 0.0223$ [28], $|\mu| < 9 \times 10^{-5}$, and $|y| < 1.2 \times 10^{-5}$ as observational limits by COBE [30,31].

B. Two-body decay

In addition, the effect of charged-lepton productions through scattering of high-energy neutrinos off background neutrinos [see Eqs. (2)–(5)] should be taken into account. The amount of energy which is converted to the background photons is estimated by

$$\frac{\Delta\rho_\gamma}{\rho_\gamma} = \int_0^\infty dt \frac{1}{\rho_\gamma} \frac{dE_l}{dt} = \frac{m_X}{2} \frac{n_X}{n_\gamma} \int_0^\infty dt \frac{1}{2.701T} \frac{1}{\tau_X} r(t, m_x, \tau_X), \tag{27}$$

where dE_l/dt is the energy density which is converted to charged lepton and finally photon through neutrino scattering per unit time and

$$r \equiv \left(\frac{m_X n_X}{2\tau_X}\right)^{-1} \frac{dE_l}{dt}. \tag{28}$$

Notice that r represents the ratio of the radiative energy injection per X decay to the X mass. The details of the calculation are found in [13,32]. In Figs. 8 and 9, we show the time evolution of r. Figure 8 shows that the ratio r increases with m_X. This is because a higher energy neutrino has a larger cross section for scattering off the background neutrino and it is also easy to exceed the threshold energy for lepton-pair creations. Similar logic applies to Fig. 9. In this case, background neutrino energy increases with the decrease of τ_X, so that the ratio r increases.

C. Constraint from CMB

As mentioned earlier, the spectral distortions are determined by $\Delta\rho_\gamma/\rho_\gamma$ which is the sum of Eqs. (20) and (27). In Figs. 10 and 11, we show the upper bounds of $m_X Y_X$ taking account of neutrino-neutrino scattering. In these figures, constraints are from the μ parameter for $\tau_X \lesssim 10^{10}$ sec and from the y parameter for $\tau_X \gtrsim 10^{10}$ sec. Consequently, there exist breaks at around $\tau_X \sim 10^{10}$ sec.

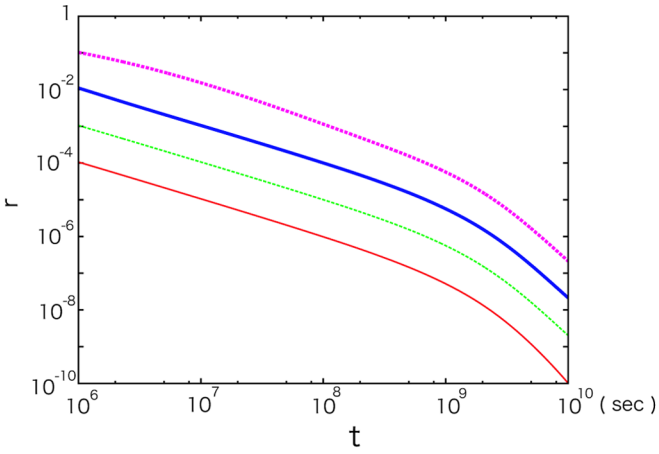

FIG. 8 (color online). The time evolution of r with $m_X = 10^2$ GeV (thin solid line), 10^3 GeV (thin dashed line), 10^4 GeV (thick solid line), and 10^5 GeV (thick dashed line). We take $\tau_X = 10^9$ sec.

When the lifetime is short and the energy of background neutrino is sufficiently high, μ is determined by neutrino-neutrino scattering, hence r. Therefore, the constraints become more severe as m_X becomes larger. When the lifetime is long, μ is determined by three- and four-body decay of X, hence $\langle E_{\rm vis}\rangle/m_X$. As already mentioned, $\langle E_{\rm vis}\rangle/m_X$ becomes smaller with larger m_X. Then, the constraints become more severe as m_X becomes smaller.

So far, we have focused only on photon energy injection. However, the emitted ultrarelativistic particles (neutrino and Y) contribute to the total relativistic energy and could lead to a more stringent constraint than that from spectral distortion, when the branching ratio is sufficiently small.

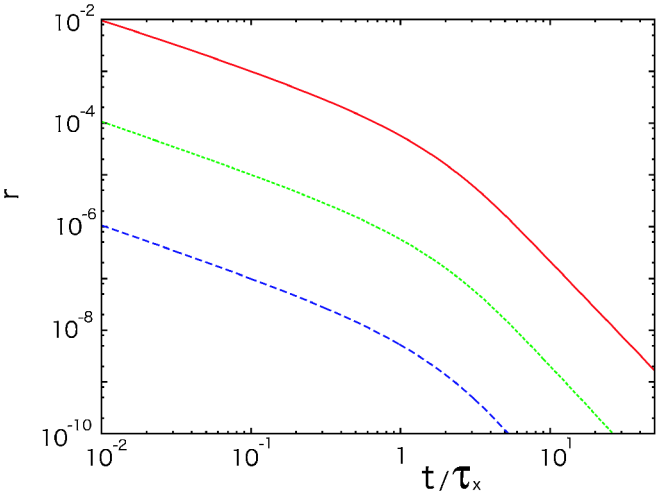

FIG. 9 (color online). The time evolution of r with $\tau_X = 10^7$ sec (solid line), 10^9 sec (dotted line), and 10^{11} sec (dashed line). We take $m_X = 10^3$ GeV.

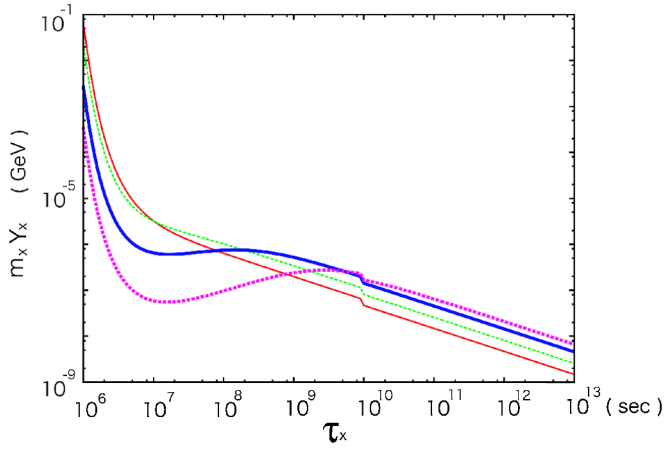

FIG. 10 (color online). CMB constraints on $m_X Y_X$ with $B_X = 10^{-3}$. From upper to lower the lines represent the upper bound of $m_X Y_X$ when $m_X = 10^2$ GeV (thin solid line), 10^3 GeV (thin dotted line), 10^4 GeV (thick solid line), and 10^5 GeV (thick dotted line).

Before recombination, the CMB angular power spectrum is sensitive to the change of the total relativistic energy through the early integrated Sachs-Wolfe effect [33]. In addition, too much relativistic energy affects the growth of large scale structure (LSS) since the epoch for the matter-radiation equality becomes later. The increase of the total relativistic energy is conventionally described by an effective number of light neutrino species ΔN_ν. The combined analysis of CMB and LSS data sets the upper bound on ΔN_ν as $\Delta N_\nu \leq 5.0$ [34]. In Fig. 12, we show the constraints from the CMB spectral distortion with $m_X = 10^3$ GeV when $B_X = 10^{-3}$ and 10^{-6}. In addition, we also show the constraint from total relativistic energy injection, which is independent of B_X. When the branching ratio is sufficiently small, Fig. 12 shows that the constraint from the total relativistic energy injection provides a more severe constraint in a wide range of lifetimes.

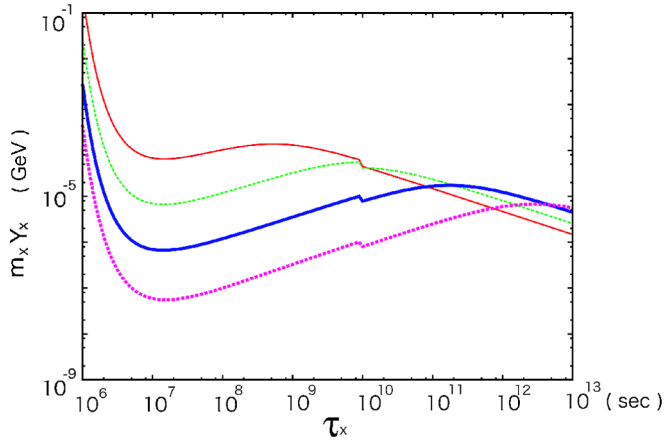

FIG. 11 (color online). Same as Fig. 10 except $B_X = 10^{-6}$.

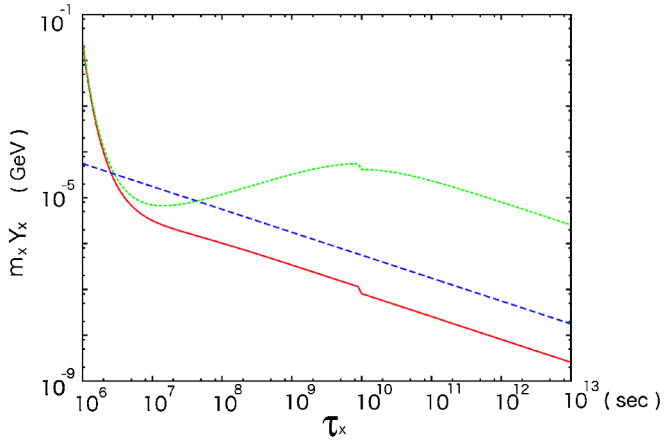

FIG. 12 (color online). Solid and dotted lines represent the CMB constraints on $m_X Y_X$ with $m_X = 1$ TeV when $B_X = 10^{-3}$ and 10^{-6} respectively. The dashed line represents the constraints from increases of the total relativistic energy.

IV. DIFFUSE NEUTRINO AND PHOTON CONSTRAINTS

A. Diffuse neutrino flux

When neutrino injection takes place very late, the emitted neutrinos may produce an observable peak in the diffuse neutrino spectrum. The present differential flux of neutrinos is given by [35,36]

$$\frac{d\Phi_\nu}{dE_0} = \frac{1}{4\pi} \int dz \frac{1}{H_0 h(z)} \frac{Y_X s_0}{\tau_X} \exp(-t/\tau_X) \frac{dN_\nu}{dE_0}, \quad (29)$$

where s_0 is the present entropy density and $h(z) = [(1+z)^3 \Omega_m + \Omega_\Lambda]^{1/2}$, with Ω_m and Ω_Λ being the density parameters of nonrelativistic matter and dark energy, respectively. Here neutrinos produced with energy E are redshifted to the observed energy $E_0 = E/(1+z)$ and E is just half of the mass of X. The source spectrum dN_ν/dE_0 is given by

$$\frac{dN_\nu(E_0)}{dE_0} = f_i \delta(E - E_0(1+z)), \quad (30)$$

where f_i is the fraction of the neutrino species $i = e, \mu, \tau$ emitted by the decay of X. (Notice that $\sum_i f_i = 1$.) We have assumed that only electron neutrinos are produced in the decay process. However, we should take the effects of neutrino oscillations into account. Neutrino oscillations can be described by six parameters: two independent mass differences $(\Delta m_{12}^2, \Delta m_{23}^2)$, three mixing angles $(\theta_{12}, \theta_{23}, \theta_{13})$ and a CP-violating phase δ. A mixing angle θ_{23} is $\sim 45°$ from atmospheric neutrino experiments [37]. A mixing angle θ_{12} is determined by solar neutrino experiments as $\theta_{12} \simeq 34°$ [38]. The CHOOZ experiment presented a mixing angle $\theta_{13} < 12°$ [39]. In our case, the neutrino traveling distance is very long and mass differences are irrelevant. The CP-violating phase δ enters the

mixing matrix only in combination with $\sin\theta_{13}$. In a reasonable approximation, $f_e \sim 0.6$ and $f_\mu \sim f_\tau \sim 0.2$ [40].

The present atmospheric neutrino $\nu_\mu + \bar{\nu}_\mu$ data gives the upper bound of the differential flux of $\nu_\mu(\bar{\nu}_\mu)$ neutrinos. The atmospheric neutrino has been observed by Super-Kamiokande [37] and AMANDA [41].[5] For observational flux of energy range $0.3 - 1.0 \times 10^3$ GeV we adopt the result in [44] where the atmospheric neutrino fluxes are estimated from the data on atmospheric neutrino event rates measured by the Super-Kamiokande experiment. For higher energy range $1.3 \times 10^3 - 3.0 \times 10^5$ GeV we use the atmospheric neutrino spectrum derived from AMANDA. In Fig. 13, we show the atmospheric neutrino fluxes from the Super-Kamiokande and AMANDA experiments as well as the diffuse neutrino fluxes from the X decay.

Futhermore, the diffuse neutrino flux is also constrained from null detection of the relic supernova $\bar{\nu}_e$ flux by Super-Kamiokande. In [45], the upper bound on $\bar{\nu}_e$ flux is obtained as $\Phi_{\bar{\nu}_e} \leq 1.2\ \mathrm{cm}^{-2}\,\mathrm{s}^{-1}$ above a threshold of $E_\nu > 19.3$ MeV.

We require that the neutrino flux from X decay should not exceed the observed atmospheric $\nu_\mu + \bar{\nu}_\mu$ flux and the upper limit of the relic supernova $\bar{\nu}_e$ flux, which leads to the constraints on the abundance of X as shown in Fig. 14. In the figure we also show the constraint from a relic supernova search only. When the lifetime is short, the constraint is very weak since the neutrinos get redshifted until the present and their energy becomes lower than the $\sim$20 MeV, which is the threshold energy of Super-Kamiokande for a relic supernova antielectron neutrino. For an intermediate lifetime, the constraints on the abundances of X are determined by the relic supernova $\bar{\nu}_e$ search and they are in proportion to m_X because the diffuse $\bar{\nu}_e$ flux is determined by the number of injected neutrinos above threshold energy, hence Y_X. When the lifetime is long, however, the constraints are determined by atmospheric neutrino fluxes. Since the neutrino flux has a peak at $\sim m_X/(1+z_d)$ (z_d: redshift at $t = \tau_X$), the maximum differential neutrino flux is proportional to Y_X/m_X. On the other hand, the observed differential neutrino flux is roughly proportional to E^{-3} and hence m_X^{-3} at $E \sim m_X$. Therefore, the constraint on $m_X Y_X$ depends on m_X as $m_X m_X^{-3}/m_X^{-1} \sim m_X^{-1}$. This means the constraints become severe with larger mass as shown in Fig. 14. Constraints for lifetimes longer than the present time t_0 scale by a factor t_0/τ_X relative to the constraints at $t_0 = \tau_X$.

B. Diffuse photon flux

High-energy photons and electrons (positrons) produced in the three- and four-body decay may be observed as diffuse gamma rays when the decay takes place after the recombination epoch. In calculating the diffuse photon spectrum, we must consider the primary photon spectrum which is not monoenergetic. In addition, we should also take account of the absorption of gamma rays along the line of sight.

Since photons are produced through three- and four-body decays, their spectrum is not monochromatic, unlike the neutrino. The energy distributions of photons, neutrinos, leptons, and nucleons produced by the three- and four-body decay of X are shown in Fig. 1. The energy of produced electrons and positrons is transferred to the background photons through the inverse Compton process. In calculating the photon flux, we have taken into account the photons produced by the inverse Compton process as well

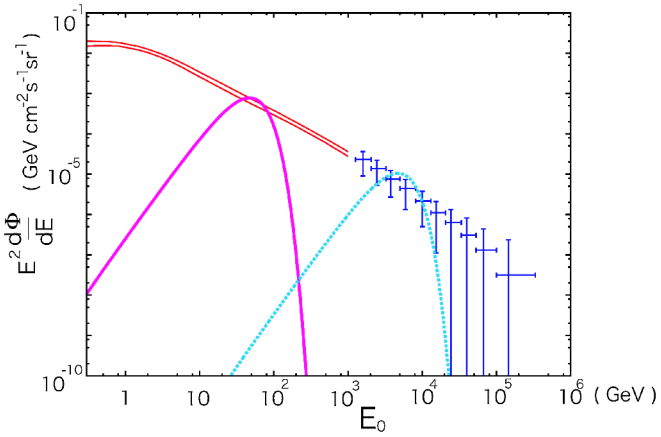

FIG. 13 (color online). Atmospheric neutrino flux. Thin solid lines represent the 1σ range of the atmospheric neutrino fluxes [44]. The point data are from AMANDA. Thick solid and dotted lines represent a diffuse neutrino signal with $m_X = 10^3$ GeV and $Y_X = 2.53 \times 10^{-17}$ (thick solid line) and 10^5 GeV and $Y_X = 3.37 \times 10^{-21}$ (thick dotted line). The lifetime is $\tau_X = 10^{16}$ sec.

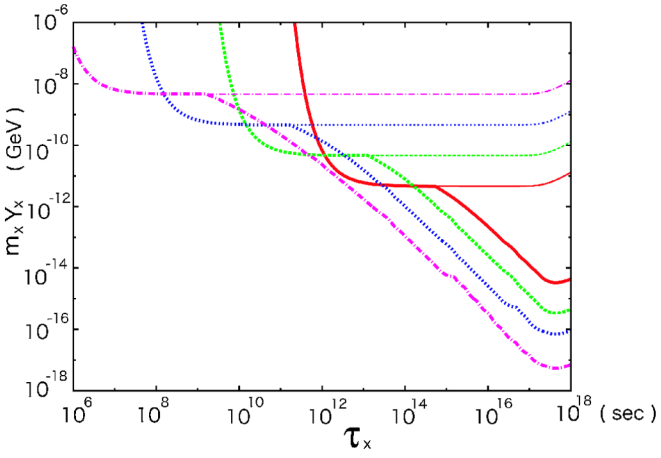

FIG. 14 (color online). Constraints from diffuse neutrino flux. From upper to lower the lines represent the upper bound of X abundance when $m_X = 10^2$ GeV (solid line), 10^3 GeV (dashed line), 10^4 GeV (dotted line), and 10^5 GeV (dot-dashed line). Thin lines are constraints only from $\bar{\nu}_e$.

[5]There are many other experiments for atmospheric neutrino, for example, [42,43].

as those from the cascade decay chain induced by the three- and four-body decay of X. The latter effect becomes more important for high-energy photons. However, since the inverse Compton process produces many soft photons, the former process becomes more significant for low-energy photons. The details of the calculation of the inverse Compton process are given in Appendix B. Nucleons are also produced in the decay, and they produce photons through the inverse Compton process or β decay. However, we neglect this effect since the number density of produced nucleons is sufficiently small. In Fig. 15, we plot the averaged photon flux (dN/dE) from one X for $m_X = 10^4$ GeV. The averaged photon flux is defined as

$$\frac{dN}{dE} = \frac{\sum_{i:\ 3,4\text{-body}} \left(\frac{dN}{dE}\right)_i \times \Gamma_i}{\sum_{i:\ 3,4\text{-body}} \Gamma_i}, \tag{31}$$

where $(dN/dE)_i$ is the photon flux in each three- and four-body decay.

High-energy photons injected in the Universe, in general, scatter through various processes: photon pair production, photon-photon scattering and pair production in matter. At the early epochs absorption and scattering due to the background photons are important, whereas significant absorption by diffuse IR-UV photons emitted from galaxies takes place at later epochs.

First let us consider the radiative processes due to the background photons. In the present case, the relevant processes are photon-photon scattering and photon pair creation [46]. Then, photons degrade their energy by producing electron-positron pairs or dividing their energy with the background photons. The photon spectrum was calculated in detail in [47]. According to [47] the present differential flux of photons is given by

$$\frac{d\Phi_\gamma}{dE_0} = \frac{1}{4\pi}\int_0^{z_*} dz \frac{1}{H_0 h(z)} \frac{Y_X s_0}{\tau_X} \exp(-t/\tau_X) \times \int dE \mathcal{L}_s(E_0(1+z), E, z)\mathcal{L}_i(E, z) B_X, \tag{32}$$

where $\mathcal{L}_i(E, z)$ is the number of photons per unit energy produced both directly and by inverse Compton at z for one X decay, and $z_*(\simeq 700)$ is the redshift at which the optical depth of high energy photons becomes 1. In addition, $\mathcal{L}_s(E_1, E_2, z)$ is the number of photons per unit energy in the spectrum when photons with energy E_1 are produced by scattering of photons with energy E_2 at redshift z. If there is no scattering, $\mathcal{L}_s(E_1, E_2, z)$ becomes $\delta(E_1 - E_2)$. (The concrete expression of $\mathcal{L}_s(E_1, E_2, z)$ is found in [47].)

In addition, γ rays with GeV to TeV energies are absorbed via electron-positron pair production on diffuse background IR-UV photons which have been emitted by galaxies [48–50]. In this paper, we adopt the result of [50], which calculated the optical depth $\tau_{\rm IR}$ of the Universe for γ rays having energies from 4 GeV to 100 TeV at redshifts from 0 to 5. (See Fig. 8 in [50].) Then the resultant photon spectrum is given by Eq. (32) multiplied by $e^{-\tau_{\rm IR}}$. We neglect the secondary soft photons produced via electron-positron pair production on diffuse background IR-UV photons, and only consider the attenuation of high-energy photons.

In Fig. 16, we show the diffuse photon flux from the COMPTEL [51] and EGRET [52] observations and decay of X, from which we obtain the upper limit on the abundance of X as shown in Fig. 17. Compared with the limit from the neutrino flux, the constraints from photon flux are almost insensitive to m_X. This can be understood as follows. The differential photon flux at the peak energy is roughly proportional to Y_X/m_X from the same reasoning as

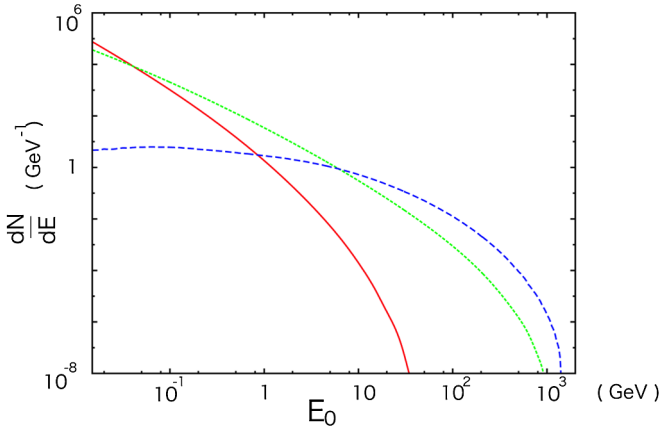

FIG. 15 (color online). Photon spectrum versus photon energy for $m_X = 10^4$ GeV. The solid line represents photons produced through the inverse Compton process at $1 + z = 1$ and the dotted line at $1 + z = 100$. The dashed line represents photons directly produced by three- and four-body decay of X.

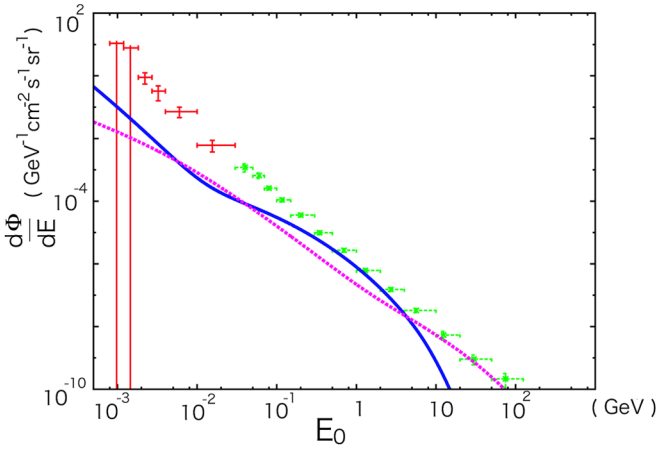

FIG. 16 (color online). Diffuse photon flux. The point data with solid error bars are from COMPTEL and the point data with dotted error bars are from EGRET. Solid and dotted lines represent the diffuse photon signal for $m_X = 10^3$ GeV and $B_X Y_X = 8.86 \times 10^{-20}$ (solid line) and 10^5 GeV and $B_X Y_X = 2.00 \times 10^{-21}$ (dotted line). The lifetime is $\tau_X = 10^{16}$ sec.

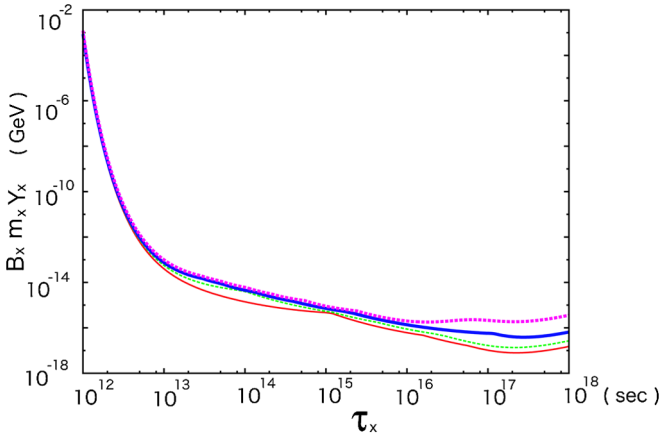

FIG. 17 (color online). Constraints from diffuse photon flux. From lower to upper the lines represent the upper bound of X abundance when $m_X = 10^2$ GeV (thin solid line), 10^3 GeV (thin dotted line), 10^4 GeV (thick solid line), and 10^5 GeV (thick dotted line).

the neutrino flux in Sec. IV A, while the observed one is proportional to $E^{-2} \propto m_X^{-2}$. Thus, the constraint on Y_X depends on m_X as $m_X^{-2} m_X \sim m_X^{-1}$, which means that the limit on $m_X Y_X$ is almost insensitive to m_X. Figure 17 shows that the constraints become less stringent with larger m_X when lifetime is long. There are two reasons for this. One is EGRET had observed up to 100 GeV. When m_X is large, the present photon energy at which the flux becomes maximum may exceed the energy range of EGRET observation. The other is higher energy photons are more effectively absorbed by diffuse background photons.

V. CONCLUSION

In this paper, we have considered the long-lived massive particle X which mainly decays into a neutrino and an invisible particle, and have investigated the cosmological and astrophysical constraints on the high-energy neutrino and photon injection due to decay of the X-particle. We have shown that the BBN, CMB, diffuse neutrino fluxes, and diffuse gamma rays provide stringent constraints on the abundance of the decaying particle X. We summarize the constraints in Figs. 18 and 19.

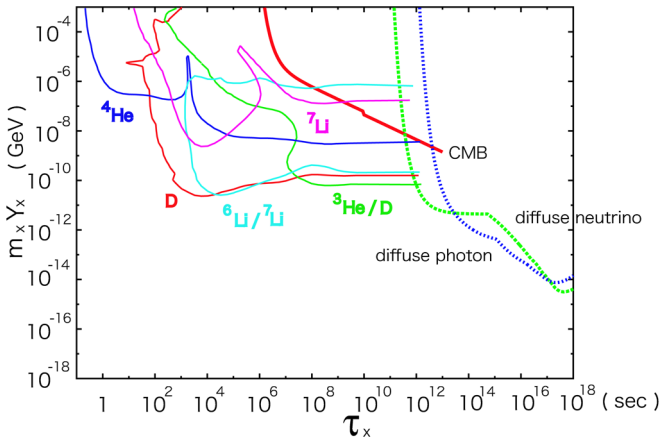

FIG. 18 (color online). The constraints on the relic abundance of X from various observations with $m_X = 100$ GeV and $B_X = 10^{-3}$.

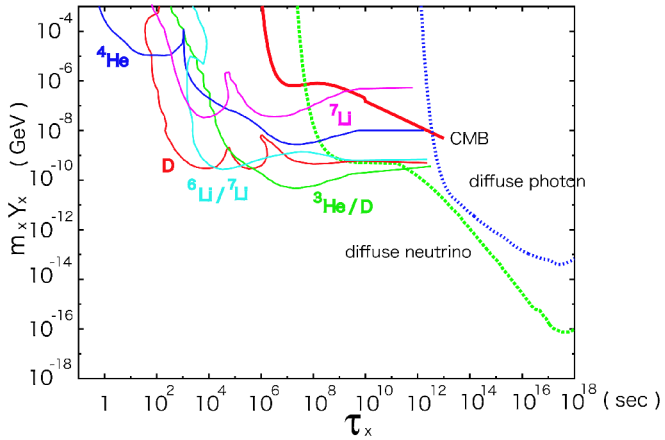

FIG. 19 (color online). The constraints on the relic abundance of X from various observations with $m_X = 10$ TeV and $B_X = 10^{-3}$.

ACKNOWLEDGMENTS

This work was supported in part by the Grant-in-Aid for Scientific Research from the Ministry of Education, Science, Sports, and Culture of Japan No. 18540254 and No. 14102004 (M. K.). This work was also supported in part by JSPS-AF Japan-Finland Bilateral Core Program (M. K.), PPARC Grant No. PP/D000394/1, EU Grant No. MRTN-CT-2006-035863, and the European Union through the Marie Curie Research and Training Network "UniverseNet," No. MRTN-CT-2006-035863 (K. K.).

APPENDIX A: BOLTZMANN EQUATION

In order to investigate effects of photo-dissociation processes and $p \leftrightarrow n$ conversion processes, we have to calculate a photon spectrum. In this paper, a source of high-energy photons is charged leptons and pions which are produced through scattering of high-energy neutrinos off background leptons. Therefore, we determine the time evolution of the distribution function of high-energy neutrinos in order to investigate the photon spectrum. In this appendix, we write down Boltzmann equations which determines the high-energy-neutrino spectrum. Our notation is the same as [32].

The high-energy neutrinos (ν) produced in X decay scatter off the thermal neutrino (ν_b) in the background by the following processes:

$$\nu_i + \nu_{i,b} \rightarrow \nu_i + \nu_i, \tag{A1}$$

$$\nu_i + \bar{\nu}_{i,b} \rightarrow \nu_i + \bar{\nu}_i, \tag{A2}$$

$$\nu_i + \bar{\nu}_{i,b} \to \nu_j + \bar{\nu}_j, \tag{A3}$$

$$\nu_i + \nu_{j,b} \to \nu_i + \nu_j, \tag{A4}$$

$$\nu_i + \bar{\nu}_{j,b} \to \nu_i + \bar{\nu}_j, \tag{A5}$$

$$\nu_i + \bar{\nu}_{i,b} \to e^- + e^+, \tag{A6}$$

$$\nu_i + \bar{\nu}_{i,b} \to \mu^- + \mu^+, \tag{A7}$$

where index i and j represent e, μ, and τ with $i \neq j$. All the amplitude squared $|\mathcal{M}|^2$ in these reactions take the following form:

$$|\mathcal{M}|^2 = 32G_F^2[a(pp')^2 + b(pq)^2 + c(pq')^2 + dm^2(pp')], \tag{A8}$$

where $G_F \simeq 1.17 \times 10^{-5}\ \mathrm{GeV}^{-2}$ is the Fermi constant, the coefficients a–d depend on the individual reaction, p and p' are the initial momenta of the high-energy-neutrino and background neutrino, q and q' are the final momenta, and m represents the mass of the fermion in the final state. Coefficients for each process are given in Table I.

First, let us consider the neutrino scattering processes Eqs. (A1)–(A5). Here, we define E_ν as the energy of the initial high-energy neutrino and E'_ν as the energy of the neutrino in the final state. We also write the distribution function of the background neutrino as

$$\bar{f}_\nu(\bar{E}_\nu) = \frac{\bar{E}_\nu^2}{2\pi^2}\frac{1}{\exp(\bar{E}_\nu/T_\nu)+1}, \tag{A9}$$

where $\bar{E}_\nu$ is the energy of background neutrino and T_ν is the neutrino temperature. We describe the contribution to the time derivative of the neutrino distribution function. When $E_\nu, E'_\nu \gg \bar{E}_\nu$, the increase of the distribution function due to scattering is written as

$$\left.\frac{\partial f_\nu(E'_\nu)}{\partial t}\right|_+ = \frac{4}{3\pi}G_F^2\int_{E'_\nu}^\infty dE_\nu \frac{1}{E_\nu^2}[aE_\nu^2 + b(E_\nu - E'_\nu)^2 + cE'^2_\nu]f_\nu(E_\nu)\int_0^\infty d\bar{E}_\nu \bar{E}_\nu \bar{f}_\nu(\bar{E}_\nu). \tag{A10}$$

On the other hand, the decrease of the neutrino distribution function is written as

$$\begin{aligned}\left.\frac{\partial f_\nu(E_\nu)}{\partial t}\right|_- &= -\frac{1}{8}\frac{1}{E_\nu^2}f_\nu(E_\nu)\int_0^\infty d\bar{E}_\nu \frac{1}{\bar{E}_\nu^2}\bar{f}_\nu(\bar{E}_\nu) \times \int_0^{4E_\nu\bar{E}_\nu} ds s\sigma(s) \\ &= -\frac{4}{3\pi}G_F^2\left(a + \frac{1}{3}b + \frac{1}{3}c\right) \times \int_0^\infty d\bar{E}_\nu \bar{E}_\nu \bar{f}_\nu(\bar{E}_\nu),\end{aligned} \tag{A11}$$

where $\sigma(s)$ is the total cross section obtained from the amplitude Eq. (A8). Notice that the condition for the neutrino number conservation is realized:

$$\int_0^\infty dE_\nu \left.\frac{\partial f_\nu(E_\nu)}{\partial t}\right|_+ = -\int_0^\infty dE_\nu \left.\frac{\partial f_\nu(E_\nu)}{\partial t}\right|_- \tag{A12}$$

unless the effects of inelastic channels ($\nu + \bar{\nu} \to e^+ + e^-, \mu^+ + \mu^-$) are taken into account.

Effects of the charged lepton-pair creation process can be taken into account in the same way, and the contribution to the time derivative of the neutrino distribution function is given by

$$\begin{aligned}\left.\frac{\partial f_\nu(E_\nu)}{\partial t}\right|_- &= -\frac{1}{8}\frac{1}{E_\nu^2}f_\nu(E_\nu)\int_0^\infty d\bar{E}_\nu \frac{1}{\bar{E}_\nu^2}\bar{f}_\nu(\bar{E}_\nu) \times \int_{4m^2}^{4E_\nu\bar{E}_\nu} ds s\sigma(s) \\ &= -\frac{1}{16\pi}G_F^2\frac{1}{E_\nu^2}f_\nu(E_\nu)\int_0^\infty d\bar{E}_\nu \frac{1}{\bar{E}_\nu^2}\bar{f}_\nu(\bar{E}_\nu) \times \left[\left(a + \frac{1}{3}b + \frac{1}{3}c\right)I_2 + \left(2d - \frac{1}{3}b - \frac{1}{3}c\right)m^2 I_1\right]\end{aligned} \tag{A13}$$

with

TABLE I. Coefficients a–d for each process. Indices i and j (with $i \neq j$) represent the generation, $\nu_{i,b}$ is the background neutrino of i-th generation, $l_i^\pm$ is the charged-lepton of i-th generation (in our case, $e^\pm$ or $\mu^\pm$). C_V and C_A are defined as follows: $C_V = -0.5 + 2\sin\theta_W^2$ and $C_A = -0.5$. Here, θ_W is the Weinberg angle.

Process	a	b	c	d
$\nu_i + \nu_{i,b} \to \nu_i + \nu_i$	2	0	0	0
$\nu_i + \bar{\nu}_{i,b} \to \nu_i + \bar{\nu}_i$	0	0	9	0
$\nu_i + \bar{\nu}_{i,b} \to \nu_j + \bar{\nu}_j$	0	0	1	0
$\nu_i + \nu_{j,b} \to \nu_i + \nu_j$	1	0	0	0
$\nu_i + \bar{\nu}_{j,b} \to \nu_i + \bar{\nu}_j$	0	0	1	0
$\nu_i + \bar{\nu}_{i,b} \to l_i^- + l_i^+$	0	$(C_V - C_A)^2$	$(C_V + C_A + 2)^2$	$(C_V - C_A)(C_V + C_A + 2)$
$\nu_i + \bar{\nu}_{i,b} \to l_j^- + l_j^+$	0	$(C_V - C_A)^2$	$(C_V + C_A)^2$	$C_V^2 - C_A^2$

$$I_2 = \frac{4}{3}\left(4 - \frac{4m^2}{E_\nu \bar{E}_\nu}\right)^{1/2} E_\nu \bar{E}_\nu (8E_\nu^2 \bar{E}_\nu^2 - 2m^2 E_\nu \bar{E}_\nu - 3m^4) - 4m^6 \ln\left[\frac{2\{4 - (4m^2/E_\nu \bar{E}_\nu)\}^{1/2} E_\nu \bar{E}_\nu + 4E_\nu \bar{E}_\nu - 2m^2}{2m^2}\right], \tag{A14}$$

$$I_1 = 2\left(4 - \frac{4m^2}{E_\nu \bar{E}_\nu}\right)^{1/2} E_\nu \bar{E}_\nu (2E_\nu \bar{E}_\nu - m^2) - 2m^4 \ln\left[\frac{2\{4 - (4m^2/E_\nu \bar{E}_\nu)\}^{1/2} E_\nu \bar{E}_\nu + 4E_\nu \bar{E}_\nu - 2m^2}{2m^2}\right]. \tag{A15}$$

Coefficients for the charged-lepton production processes are given in Table I.

In addition, there are processes for neutrino scattering as follows:

$$\nu_e + \bar{\nu}_{\mu,b} \to \mu^+ + e^-, \tag{A16}$$

$$\nu_\mu + \bar{\nu}_{e,b} \to \mu^- + e^+. \tag{A17}$$

The amplitudes squared in these reactions take the form given by

$$|\mathcal{M}|^2_{\nu_e + \bar{\nu}_{\mu,b} \to \mu^+ + e^-} = 128 G_F^2 (pq')\left[(pq') - \frac{1}{2}(m_\mu^2 - m_e^2)\right], \tag{A18}$$

$$|\mathcal{M}|^2_{\nu_\mu + \bar{\nu}_{e,b} \to \mu^- + e^+} = 128 G_F^2 (pq')\left[(pq') + \frac{1}{2}(m_\mu^2 - m_e^2)\right]. \tag{A19}$$

Effects of these process can be taken into account in the same way. However, it is somewhat complicated to calculate Boltzmann equations for these processes due to the mass difference between the muon and electron. The contributions to the time derivative of the neutrino distribution function are given by

$$\left.\frac{f_{\nu_e}(E_\nu)}{\partial t}\right|_{\nu_e + \bar{\nu}_{\mu,b} \to \mu^+ + e^-} = \left.\frac{f_{\nu_\mu}(E_\nu)}{\partial t}\right|_{\nu_\mu + \bar{\nu}_{e,b} \to \mu^- + e^+} = -\frac{G_F^2}{24\pi} E_\nu f_\nu(E_\nu) \times \int_0^\infty d\bar{E}_\nu \bar{f}_\nu(\bar{E}_\nu) I_3, \tag{A20}$$

with

$$I_3 = \frac{z}{3}[-5x^2 - 2xy - 5y^2 - 20(x + y) + 64] + (x^3 - 3x^2 y - 3xy^2 + y^3)\ln\left[\frac{4 - x - y + 2z}{2\sqrt{xy}}\right] + |x - y|^3 \ln\left[\frac{4(x + y) - (x - y)^2 - 2z|x - y|}{8\sqrt{xy}}\right], \tag{A21}$$

where $x = m_\mu^2/E_\nu \bar{E}_\nu$, $y = m_e^2/E_\nu \bar{E}_\nu$, and $z = [4 - 2(x + y) + \frac{1}{4}(x - y)^2]^{1/2}$.

Finally, we consider the effect of the charged pion pair creation process. The cross section for charged pion pair production is given by

$$\sigma(\nu\bar{\nu} \to \pi^+ \pi^-) = \frac{1}{12\pi} G_F^2 (1 - 2\sin^2\theta_W)^2 s \times \left(1 - \frac{4m_\pi^2}{s}\right)^{3/2} |F(s)|^2 \tag{A22}$$

with

$$|F(s)|^2 = \frac{m_\rho^4}{(s - m_\rho^2)^2 + m_\rho^2 \Gamma_\rho^2}, \tag{A23}$$

where m_ρ and Γ_ρ are the mass and decay width of the ρ meson, respectively [53]. The contribution to the time derivative of the neutrino distribution function is given by Eq. (A13) and the cross section above.

Next, we turn now to neutrino-electron scattering processes. The high-energy neutrinos also scatter off the thermal electron (e_b^-) and positron (e_b^+) by the following processes:

$$\nu_e + e_b^- \to \nu_e + e^-, \tag{A24}$$

$$\nu_e + e_b^+ \to \nu_e + e^+, \tag{A25}$$

$$\nu_i + e_b^- \to \nu_i + e^-, \tag{A26}$$

$$\nu_i + e_b^+ \to \nu_i + e^+, \tag{A27}$$

where index i represents μ and τ. All the amplitude squared in these reactions take the same form as Eq. (A8). In this case, however, p and q are the initial and final momenta of the neutrino and p' and q' are that of the background electron (positron). Coefficients for each process are given in Table II. We write the distribution function of the background electron (positron) as

$$\bar{f}_e(\bar{E}_e) = \frac{\bar{p}_e^2}{2\pi^2} \frac{1}{\exp(\bar{E}_e/T_\gamma) + 1} \tag{A28}$$

where $\bar{E}_e$ and $\bar{p}_e$ are the energy and momentum of background electron (positron), respectively. Photon temperature T_γ is different from neutrino temperature T_ν due to neutrino decoupling and subsequent electron-positron pair annihilation. From entropy conservation, the relation between them is given by

$$T_\nu = \left(\frac{4}{11}\right)^{1/3} T_\gamma \left[1 + \frac{45}{2\pi^2}\frac{1}{T_\gamma^4} \times \int_0^\infty d\bar{p}_e \left(\bar{E}_e + \frac{\bar{p}_e^2}{3\bar{E}_e}\right)\bar{f}_e(\bar{E}_e)\right]^{1/3}. \tag{A29}$$

TABLE II. Coefficients a–d for each process. Index i represents μ and τ; e_b is the background electron and positron.

Process	a	b	c	d
$\nu_e + e_b^- \to \nu_e + e^-$	$(C_V + C_A + 2)^2$	0	$(C_V - C_A)^2$	$-(C_V - C_A)(C_V + C_A + 2)$
$\nu_e + e_b^+ \to \nu_e + e^+$	$(C_V - C_A)^2$	0	$(C_V + C_A + 2)^2$	$-(C_V - C_A)(C_V + C_A + 2)$
$\nu_i + e_b^- \to \nu_i + e^-$	$(C_V + C_A)^2$	0	$(C_V - C_A)^2$	$-(C_V^2 - C_A^2)$
$\nu_i + e_b^+ \to \nu_i + e^+$	$(C_V - C_A)^2$	0	$(C_V + C_A)^2$	$-(C_V^2 - C_A^2)$

The effects of neutrino-electron scattering are only important at early time because of the Boltzmann suppression of the distribution function of the background electron (positron). When $E_\nu, E'_\nu \gg \bar{E}_e$, the increase and decrease of the distribution functions are given by

$$\left.\frac{\partial f_\nu(E'_\nu)}{\partial t}\right|_+ = \frac{4}{3\pi} G_F^2 \int_{E'_\nu}^\infty dE_\nu \frac{1}{E_\nu^2}[aE_\nu^2 + b(E_\nu - E'_\nu)^2 + cE'^2{}_\nu] f_\nu(E_\nu) \int_0^\infty d\bar{p}_e \bar{E}_e \bar{f}_e(\bar{E}_e)\left(1 - \frac{m_e^2}{4\bar{E}_e^2}\right), \tag{A30}$$

$$\begin{aligned}\left.\frac{\partial f_\nu(E_\nu)}{\partial t}\right|_- &= -\frac{1}{8}\frac{1}{E_\nu^2} f_\nu(E_\nu) \int_0^\infty d\bar{p}_e \frac{1}{\bar{p}_e \bar{E}_e} \bar{f}_e(\bar{E}_e) \\ &\quad \times \int ds (s - m_e^2)\sigma(s) \\ &= -\frac{4}{3\pi} G_F^2 \left(a + \frac{1}{3}b + \frac{1}{3}c\right) E_\nu f_\nu(E_\nu) \\ &\quad \times \int_0^\infty d\bar{p}_e \bar{E}_e \bar{f}_e(\bar{E}_e)\left(1 - \frac{m_e^2}{4\bar{E}_e^2}\right).\end{aligned} \tag{A31}$$

Notice that the condition for the neutrino number conservation is also realized just as neutrino-neutrino scattering.

We also include the following process:

$$\nu_\mu + e^- \to \nu_e + \mu^-. \tag{A32}$$

The amplitude squared in this reaction is given by

$$|\mathcal{M}|^2_{\nu_\mu + e^- \to \nu_e + \mu^-} = 128 G_F^2 (pp')\left[(pp') - \frac{1}{2}(m_\mu^2 - m_e^2)\right]. \tag{A33}$$

For simplicity, we neglect the mass difference between the muon and electron in this reaction. On this assumption, this process is the same form as $\nu_i + e \to \nu_i + e$.

In addition, we consider the effect of the pion pair creation process. The cross section for pion pair production is given by

$$\sigma(\bar{\nu}_e e^- \to \pi^- \pi^0) = \frac{1}{12\pi} G_F^2 s \left(1 - \frac{4m_\pi^2}{s}\right)^{3/2} |F(s)|^2, \tag{A34}$$

where $|F(s)|^2$ is defined in Eq. (A23) [53]. The contribution to the time derivative of the neutrino distribution function is given by Eq. (A31) with the cross section above.

Then one can obtain the Boltzmann equations describing the evolution of the spectra for the high-energy neutrinos:

$$\begin{aligned}\frac{\partial f_{\nu_i}(E'_\nu)}{\partial t} &= \frac{4G_F^2}{3\pi} \int_{E'_\nu}^\infty dE_\nu \frac{1}{E_\nu^2} \sum_j [a^\nu_{\text{in},ij} E_\nu^2 + b^\nu_{\text{in},ij}(E_\nu - E'_\nu)^2 + c^\nu_{\text{in},ij} E'^2{}_\nu] f_{\nu_j}(E_\nu) \int_0^\infty d\bar{E}_\nu \bar{E}_\nu \bar{f}_\nu(\bar{E}_\nu) \\ &\quad - \frac{4G_F^2}{3\pi} E'_\nu f_{\nu_i}(E'_\nu)\left(a^\nu_{\text{out}} + \frac{1}{3}b^\nu_{\text{out}} + \frac{1}{3}c^\nu_{\text{out}}\right) \int_0^\infty d\bar{E}_\nu \bar{E}_\nu \bar{f}_\nu(\bar{E}_\nu) + \frac{4G_F^2}{3\pi} \int_{E'_\nu}^\infty dE_\nu \frac{1}{E_\nu^2}[a^e_{\text{in},i} E_\nu^2 + b^e_{\text{in},i}(E_\nu - E'_\nu)^2 \\ &\quad + c^e_{\text{in},i} E'^2{}_\nu] f_{\nu_i}(E_\nu) \int_0^\infty d\bar{p}_e \bar{E}_e \bar{f}_e(\bar{E}_e)\left(1 - \frac{1}{4}\frac{m_e^2}{\bar{E}_e^2}\right) - \frac{4G_F^2}{3\pi} E'_\nu f_{\nu_i}(E'_\nu)\left(a^e_{\text{out},i} + \frac{1}{3}b^e_{\text{out},i} + \frac{1}{3}c^e_{\text{out},i}\right) \\ &\quad \times \int_0^\infty d\bar{p}_e \bar{E}_e \bar{f}_e(\bar{E}_e)\left(1 - \frac{1}{4}\frac{m_e^2}{\bar{E}_e^2}\right) + \left(\frac{\partial f_{\nu_i}(E'_\nu)}{\partial t}\right)_{\nu_i + \bar{\nu}_i \to e^- + e^+} + \left(\frac{\partial f_{\nu_i}(E'_\nu)}{\partial t}\right)_{\nu_i + \bar{\nu}_i \to \mu^- + \mu^+} \\ &\quad + \left(\frac{\partial f_{\nu_e}(E'_\nu)}{\partial t}\right)_{\nu_e + \bar{\nu}_\mu \to e^- + \mu^+} \delta_{i,e} + \left(\frac{\partial f_{\nu_\mu}(E'_\nu)}{\partial t}\right)_{\nu_\mu + \bar{\nu}_e \to \mu^- + e^+} \delta_{i,\mu} + \left(\frac{\partial f_{\nu_e}(E'_\nu)}{\partial t}\right)_{\nu_\mu + e^- \to \nu_e + \mu^-} \delta_{i,e} \\ &\quad + \left(\frac{\partial f_{\nu_\mu}(E'_\nu)}{\partial t}\right)_{\nu_\mu + e^- \to \nu_e + \mu^-} \delta_{i,\mu} + \left(\frac{\partial f_{\nu_i}(E'_\nu)}{\partial t}\right)_{\nu_i + \bar{\nu}_i \to \pi^+ + \pi^-} + \left(\frac{\partial f_{\nu_e}(E'_\nu)}{\partial t}\right)_{\nu_e + e^+ \to \pi^+ + \pi^0} \delta_{i,e} \\ &\quad + \frac{1}{2\tau_X} n_X \delta(E'_\nu - m_X/2)\delta_{i,e} + E'_\nu H \frac{\partial f_{\nu_i}(E'_\nu)}{\partial E'_\nu} - 2H f_{\nu_i}(E'_\nu),\end{aligned} \tag{A35}$$

where H is the expansion rate of the Universe and $\delta_{i,j}$ is a Kronecker delta. The coefficients for neutrino-neutrino scattering are given by

$$a^{\nu}_{\rm out} = 4, \qquad b^{\nu}_{\rm out} = 0, \qquad c^{\nu}_{\rm out} = 13, \tag{A36}$$

$$a^{\nu}_{{\rm in},ii} = 6, \qquad b^{\nu}_{{\rm in},ii} = 9, \qquad c^{\nu}_{{\rm in},ii} = 11, \tag{A37}$$

$$a^{\nu}_{{\rm in},ij} = 1, \qquad b^{\nu}_{{\rm in},ij} = 1, \qquad c^{\nu}_{{\rm in},ij} = 2, \qquad (i \neq j). \tag{A38}$$

For example, let us derive $a^{\nu}_{\rm out}$. Factor 2 comes from $\nu_i\nu_i \rightarrow \nu_i\nu_i$ scattering and another factor 2 comes from $\nu_i\nu_j \rightarrow \nu_i\nu_j$ scattering. Consequently, the coefficient $a^{\nu}_{\rm out}$ amounts to 4. Other coefficients can be derived in the same manner. The coefficients for neutrino-electron scattering are given by

$$\begin{aligned} &a^{e}_{{\rm out},e} = (C_V + C_A + 2)^2 + (C_V - C_A)^2, \\ &b^{e}_{{\rm out},e} = 0,\ c^{e}_{{\rm out},e} = a^{e}_{{\rm out},e}, \end{aligned} \tag{A39}$$

$$\begin{aligned} &a^{e}_{{\rm out},j} = (C_V + C_A)^2 + (C_V - C_A)^2, \\ &b^{e}_{{\rm out},j} = 0, \qquad c^{e}_{{\rm out},j} = a^{e}_{{\rm out},j}, \end{aligned} \tag{A40}$$

$$a^{e}_{{\rm in},i} = a^{e}_{{\rm out},i}, \qquad b^{e}_{{\rm in},i} = b^{e}_{{\rm out},i}, \qquad c^{e}_{{\rm in},i} = c^{e}_{{\rm out},i}, \tag{A41}$$

where the index i represents e, μ, and τ and j represents μ and τ.

APPENDIX B: INVERSE COMPTON

In this appendix, we write down Boltzmann equations for the inverse Compton process which determines the high-energy photon spectrum. The electron energies before scattering and after scattering are given by E_e and E'_e. E_γ is used for the energy of the scattered photon and ϵ_γ for the background photon.

The diffuse extragalactic γ ray flux has been observed by the COMPTEL and EGRET measurements. COMPTEL and EGRET observed γ ray energy ranges from 0.8 MeV to 100 GeV. Electrons and positrons which scatter up background photons to this energy range should be highly relativistic. Thus, the number of collisions per unit time per photon energy through the inverse Compton process is written as [54]

$$\frac{d^2N}{dtdE_\gamma}(\epsilon_\gamma, E_\gamma, E_e) = 8\pi r_e^2 \frac{1}{\Gamma E_e}\Big(2q\ln q + (1+2q) \times (1-q) + \frac{1}{2}\frac{(\Gamma q)^2}{1+\Gamma q}(1-q)\Big), \tag{B1}$$

where r_e is the classical electron radius, $\Gamma = 4\epsilon_\gamma E_e/m_e^2$, and $q = E_\gamma/\Gamma(E_e - E_\gamma)$. The maximum photon energy is given by $E_e\Gamma/(1+\Gamma)$.

The Boltzmann equations for the inverse Compton process are given by

$$\frac{\partial f_\gamma(E_\gamma)}{\partial t} = \int_{(E_\gamma/2)(1+\sqrt{1+4/\Gamma})}^{\infty} dE_e f_e(E_e) \int_0^\infty d\epsilon_\gamma f_b(\epsilon_\gamma) \times \frac{d^2N}{dtdE_\gamma}(\epsilon_\gamma, E_\gamma, E_e), \tag{B2}$$

$$\frac{\partial f_e(E'_e)}{\partial t} = \int_{E'_e}^{E_{\rm max}} dE_e f_e(E_e) \int_0^\infty d\epsilon_\gamma f_b(\epsilon_\gamma) \frac{d^2N}{dtdE_\gamma} \times (\epsilon_\gamma, E_\gamma = E_e + \epsilon_\gamma - E'_e, E_e) - f_e(E'_e) \times \int_0^\infty d\epsilon_\gamma f_b(\epsilon_\gamma) \frac{dN}{dt}(\epsilon_\gamma, E'_e), \tag{B3}$$

where $E_{\rm max} = m_e{}^2(E'_e - \epsilon_\gamma)/(4\epsilon_\gamma{}^2 + m_e{}^2 - 4\epsilon_\gamma E'_e)$ when the denominator is positive and $E_{\rm max} = \infty$ when negative. The distribution function of the background photons at temperature T_γ is represented by $f_b(\epsilon_\gamma)$,

$$f_b(\epsilon_\gamma) = \frac{\epsilon_\gamma{}^2}{\pi^2}\frac{1}{\exp(\epsilon_\gamma/T_\gamma) - 1}. \tag{B4}$$

To check the validity of these Boltzmann equations, we show the electron number conservation:

$$\begin{aligned} \int_{m_e}^\infty dE'_e \frac{\partial f_e(E'_e)}{\partial t} &= \int_{m_e}^\infty dE_e f_e(E_e) \int_{E_e/(1+\Gamma)+\epsilon_\gamma}^{E_e} dE'_e \int_0^\infty d\epsilon_\gamma f_b(\epsilon_\gamma) \frac{d^2N}{dtdE_\gamma}(\epsilon_\gamma, E_e + \epsilon_\gamma - E'_e, E_e) \\ &\quad - \int_{m_e}^\infty dE'_e f_e(E'_e) \int_0^\infty d\epsilon_\gamma f_b(\epsilon_\gamma) \frac{dN}{dt}(\epsilon_\gamma, E'_e) \\ &= \int_{m_e}^\infty dE_e f_e(E_e) \int_{\epsilon_\gamma}^{E_e\Gamma/(1+\Gamma)} dE_\gamma \int_0^\infty d\epsilon_\gamma f_b(\epsilon_\gamma) \frac{d^2N}{dtdE_\gamma}(\epsilon_\gamma, E_\gamma, E_e) \\ &\quad - \int_{m_e}^\infty dE'_e f_e(E'_e) \int_0^\infty d\epsilon_\gamma f_b(\epsilon_\gamma) \frac{dN}{dt}(\epsilon_\gamma, E'_e) \\ &= \int_{m_e}^\infty dE_e f_e(E_e) \int_0^\infty d\epsilon_\gamma f_b(\epsilon_\gamma) \frac{dN}{dt}(\epsilon_\gamma, E_e) - \int_{m_e}^\infty dE'_e f_e(E'_e) \int_0^\infty d\epsilon_\gamma f_b(\epsilon_\gamma) \frac{dN}{dt}(\epsilon_\gamma, E'_e) = 0. \end{aligned}$$

The energy conservation is also easily shown:

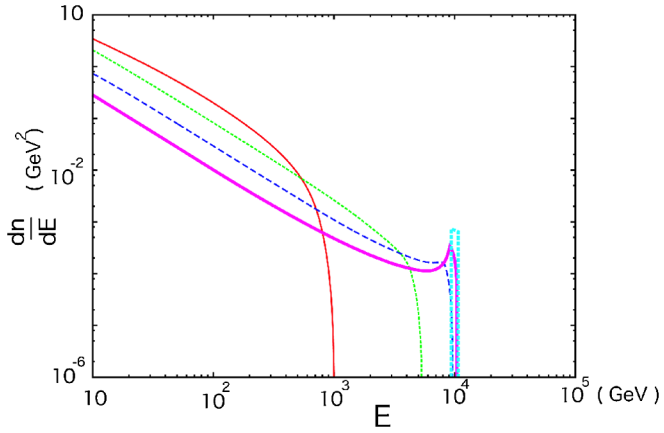

FIG. 20 (color online). Photon spectra which are produced through the inverse Compton process when high-energy electrons are injected with $E_e = 10^4$ GeV and $n_e = 1$ GeV^3. From upper to lower the lines represent the photon spectra when $1 + z = 1$ (thin solid line), 10 (thin dotted line), 100 (thin dashed line), and 1000 (thick solid line). The thick dotted line represents the initial electron spectrum. For simplicity, we have assumed here that the background photon spectrum is monochromatic with $\epsilon_\gamma = 2.7T_\gamma$

$$\int_{\epsilon_\gamma}^{\infty} dE_\gamma (E_\gamma - \epsilon_\gamma) \frac{\partial f_\gamma(E_\gamma)}{\partial t} = \int_{m_e}^{\infty} dE_e f_e(E_e) \int_0^{\infty} d\epsilon_\gamma f_b(\epsilon_\gamma) \int_{\epsilon_\gamma}^{E_e\Gamma/(1+\Gamma)} dE_\gamma (E_\gamma - \epsilon_\gamma) \frac{d^2N}{dtdE_\gamma}(\epsilon_\gamma, E_\gamma, E_e),$$

$$\int_{m_e}^{\infty} dE'_e E'_e \frac{\partial f_e(E'_e)}{\partial t} = \int_{m_e}^{\infty} dE_e f_e(E_e) \int_0^{\infty} d\epsilon_\gamma f_b(\epsilon_\gamma) \int_{\epsilon_\gamma}^{E_e\Gamma/(1+\Gamma)} dE_\gamma (E_e + \epsilon_\gamma - E_\gamma) \frac{d^2N}{dtdE_\gamma}(\epsilon_\gamma, E_\gamma, E_e)$$

$$- \int_{m_e}^{\infty} dE'_e E'_e f_e(E'_e) \int_0^{\infty} d\epsilon_\gamma f_b(\epsilon_\gamma) \frac{dN}{dt}(\epsilon_\gamma, E'_e) = - \int_{\epsilon_\gamma}^{\infty} dE_\gamma (E_\gamma - \epsilon_\gamma) \frac{\partial f_\gamma(E_\gamma)}{\partial t}.$$

In Fig. 20, we plot the photon spectra which are produced through the inverse Compton process when high-energy electrons are injected. The photon spectra have quite a different form for different values of Γ. In the Thomson limit corresponding to $\Gamma \ll 1$, the first two terms of the right-hand side of Eq. (B1) are dominant. In this case, many low-energy photons are produced. In the extreme Klein-Nishina limit corresponding to $\Gamma \gg 1$, the last term of the right-hand side of Eq. (B1) is dominant at larger q and the photon spectra have peaks near the high-energy end [55]. Our calculation is different from the steady-state method [55,56]. However, once the electron spectrum is in a steady-state, our result is in good agreement with the result in [55,56].

[1] J. C. Mather *et al.*, Astrophys. J. **420**, 439 (1994).
[2] D. Lindley, Astrophys. J. **294**, 1 (1985); M. Y. Khlopov and A. D. Linde, Phys. Lett. **138B**, 265 (1984); J. R. Ellis, J. E. Kim, and D. V. Nanopoulos, Phys. Lett. **145B**, 181 (1984); R. Juszkiewicz, J. Silk, and A. Stebbins, Phys. Lett. **158B**, 463 (1985); J. R. Ellis, D. V. Nanopoulos, and S. Sarkar, Nucl. Phys. **B259**, 175 (1985); J. Audouze, D. Lindley, and J. Silk, Astrophys. J. **293**, L53 (1985); D. Lindley, Phys. Lett. B **171**, 235 (1986); M. Kawasaki and K. Sato, Phys. Lett. B **189**, 23 (1987); R. J. Scherrer and M. S. Turner, Astrophys. J. **331**, 19 (1988); J. R. Ellis *et al.*, Nucl. Phys. **B373**, 399 (1992).
[3] M. Kawasaki and T. Moroi, Prog. Theor. Phys. **93**, 879 (1995); Astrophys. J. **452**, 506 (1995).
[4] E. Holtmann, M. Kawasaki, K. Kohri, and T. Moroi, Phys. Rev. D **60**, 023506 (1999).
[5] K. Jedamzik, Phys. Rev. Lett. **84**, 3248 (2000); M. Kawasaki, K. Kohri, and T. Moroi, Phys. Rev. D **63**, 103502 (2001); R. H. Cyburt, J. R. Ellis, B. D. Fields, and K. A. Olive, Phys. Rev. D **67**, 103521 (2003).
[6] R. Dominguez-Tenreiro, Astrophys. J. **313**, 523 (1987).
[7] M. H. Reno and D. Seckel, Phys. Rev. D **37**, 3441 (1988).
[8] S. Dimopoulos *et al.*, Astrophys. J. **330**, 545 (1988); Nucl. Phys. **B311**, 699 (1989).
[9] K. Kohri, Phys. Rev. D **64**, 043515 (2001).
[10] M. Kawasaki, K. Kohri, and T. Moroi, Phys. Lett. B **625**, 7 (2005); Phys. Rev. D **71**, 083502 (2005).
[11] K. Kohri, T. Moroi, and A. Yotsuyanagi, Phys. Rev. D **73**, 123511 (2006).
[12] K. Jedamzik, Phys. Rev. D **74**, 103509 (2006).
[13] M. Kawasaki and T. Moroi, Phys. Lett. B **346**, 27 (1995)
[14] J. L. Feng, S.-f. Su, and F. Takayama, Phys. Rev. D **70**, 063514 (2004); Phys. Rev. D **70**, 075019 (2004).
[15] T. Kanzaki, M. Kawasaki, K. Kohri, and T. Moroi, Phys.

Rev. D **75**, 025011 (2007).
[16] P. Gondolo, G. Gelmini, and S. Sarkar, Nucl. Phys. **B392**, 111 (1993).
[17] T. Sjostrand *et al.*, Comput. Phys. Commun. **135**, 238 (2001).
[18] L. H. Kawano, FERMILAB Report No. FERMILAB-Pub-92/04-A, 1992.
[19] Y. I. Izotov, T. X. Thuan, and G. Stasinska, arXiv:astro-ph/0702072.
[20] M. Peimbert, V. Luridiana, and A. Peimbert, arXiv:astro-ph/0701580.
[21] M. Fukugita and M. Kawasaki, Astrophys. J. **646**, 691 (2006).
[22] J. Geiss and G. Gloeckler, Space Sci. Rev. **106**, 3 (2003).
[23] G. Sigl, K. Jedamzik, D. N. Schramm, and V. S. Berezinsky, Phys. Rev. D **52**, 6682 (1995).
[24] J. Silk and A. Stebbins, Astrophys. J. **269**, 1 (1983).
[25] M. Kawasaki and K. Sato, Phys. Lett. **169B**, 280 (1986).
[26] W. Hu and J. Silk, Phys. Rev. Lett. **70**, 2661 (1993).
[27] G. Steigman, Int. J. Mod. Phys. E **15**, 1 (2006).
[28] D. N. Spergel *et al.*, Astrophys. J. Suppl. Ser. **170**, 377 (2007).
[29] L. Danese and G. De Zotti, Astron. Astrophys. **107**, 39 (1982).
[30] D. J. Fixsen, E. S. Cheng, J. M. Gales, J. C. Mather, R. A. Shafer, and E. L. Wright, Astrophys. J. **473**, 576 (1996)
[31] K. Hagiwara *et al.* (Particle Data Group), Phys. Rev. D **66**, 010001 (2002).
[32] T. Moroi, arXiv:hep-ph/9503210.
[33] A. R. Zentner and T. P. Walker, Phys. Rev. D **65**, 063506 (2002).
[34] K. Ichikawa, M. Kawasaki, and F. Takahashi, J. Cosmol. Astropart. Phys. 05 (2007) 007.
[35] L. Bergstrom, J. Edsjo, and P. Ullio, Phys. Rev. Lett. **87**, 251301 (2001).
[36] J. F. Beacom, N. F. Bell, and G. D. Mack, arXiv:astro-ph/0608090.
[37] Y. Ashie *et al.*, Phys. Rev. D **71**, 112005 (2005).
[38] B. Aharmim *et al.*, Phys. Rev. C **72**, 055502 (2005).
[39] M. Apollonio *et al.*, Eur. Phys. J. C **27**, 331 (2003).
[40] M. L. Costantini and F. Vissani, Astropart. Phys. **23**, 477 (2005).
[41] H. Geenen (AMANDA Collaboration), "Atmospheric neutrino and muon spectra measured with the AMANDA-II detector," in Proceedings of the 28th International Cosmic Ray Conferences (ICRC), Tsukuba, Japan, 2003.
[42] G. Giacomelli and A. Margiotta, Phys. At. Nucl. **67**, 1139 (2004).
[43] M. C. Sanchez *et al.*, Phys. Rev. D **68**, 113004 (2003).
[44] M. C. Gonzalez-Garcia, M. Maltoni, and J. Rojo, J. High Energy Phys. 10 (2006) 075.
[45] M. Malek *et al.*, Phys. Rev. Lett. **90**, 061101 (2003).
[46] A. A. Zdziarski and R. Svensson, Astrophys. J. **344**, 551 (1989).
[47] G. D. Kribs and I. Z. Rothstein, Phys. Rev. D **55**, 4435 (1997).
[48] M. H. Salamon and F. W. Stecker, Astrophys. J. **493**, 547 (1998).
[49] J. R. Primack, R. J. Somerville, J. S. Bullock, and J. E. G. Devriendt, AIP Conf. Proc. **558**, 463 (2001).
[50] F. W. Stecker, M. A. Malkan, and S. T. Scully, Astrophys. J. **648**, 774 (2006); see also F. W. Stecker, M. A. Malkan, and S. T. Scully, Astrophys. J. **658**, 1392 (2007).
[51] S. C. Kappadath *et al.*, Astron. Astrophys. Suppl. Ser. **120**, 619 (1996); P. Sreekumar, F. W. Stecker, and S. C. Kappadath, AIP Conf. Proc. **510**, 459 (2000).
[52] P. Sreekumarand *et al.*, Astrophys. J. **494**, 523 (1998).
[53] See, for example, R. P. Feynman, *Photon-Hadron Interactions* (W. A. Benjamin, Massachusetts, 1972).
[54] F. C. Jones, Phys. Rev. **167**, 1159 (1968).
[55] G. R. Blumenthal and R. J. Gould, Rev. Mod. Phys. **42**, 237 (1970).
[56] G. R. Blumenthal, Phys. Rev. D **3**, 2308 (1971).